Sea Ice
Part II. Estimating the Full-Scale Tensile, Flexural, and Compressive Strength of First-Year Ice

Austin Kovacs   September 1996

$$\sigma_C = 1970\dot{\varepsilon}^{0.32}\,\phi_B^{-0.95}$$
$$r^2 = 0.941$$
$$S\,D = 0.25$$

Abstract: Sea-ice salinity, density, and temperature data were used to develop new methods for determining the bulk brine volume and porosity of sea-ice floes. Methods for estimating full-thickness ice sheet strength, based on large-scale field tests, are presented. The relationships among bulk sea-ice properties, strain rate, and strength are illustrated. A new constitutive equation was developed for predicting the full-thickness horizontal compressive strength σ_c of first-year sea ice as a function of the applied strain rate and bulk porosity in the form $\sigma_c = B_2 \, \dot{\varepsilon}^{1/n} \, \phi_B^m$, where parameters B_2, n, and m are about 2.7×10^3, 3, and -1, respectively, and $\dot{\varepsilon}$ and ϕ_B are the ice strain rate and ice floe bulk porosity of sea ice, respectively. An estimate of the horizontal force that may develop between first-year sea ice and a 90-m-wide structure is given. Estimating sea-ice strength based on remote ice conductivity measurements is also discussed conceptually.

Cover: Exxon ice floe σ_c values vs. bulk porosity and strain rate.

CRREL Report 96-11

Sea Ice
Part II. Estimating the Full-Scale Tensile, Flexural, and Compressive Strength of First-Year Ice

Austin Kovacs   September 1996

19961113 043

PREFACE

CONTENTS

ILLUSTRATIONS

Sea Ice
Part II. Estimating the Full-Scale Tensile, Flexural, and Compressive Strength of First-Year Ice

AUSTIN KOVACS

INTRODUCTION

It is well known that the strength of sea ice is to a large extent dependent on brine volume, and that brine volume is a function of ice salinity and temperature. Brine volume may be estimated using the empirical expressions of Frankenstein and Garner (1967) or the theoretical density–volume fraction equations of Cox and Weeks (1983). The former is by far the simplest method, because the only inputs required in the brine volume equations are ice salinity and temperature. Since the latter approach is based on phase relationships, it allows for the calculation of the gas volume and thus the total ice porosity and the brine-free ice density. With this method, the bulk density of the sea ice is also needed and therefore must be determined. In principle this is a simple task, but it can be difficult to do in the field. Today, ice core weight is measured by electronic scales rather than triple beam balances, which are subject to uneven support surface and wind effect errors when used at unsheltered sites. Electronic scale weight measurements can be highly representative of the in-situ ice if brine drainage has not occurred during coring or after the ice core was removed from the bore hole. Determining ice core volume is a bit more troublesome. Ice core length should be measured along the center axis using a special caliper or gauging device (Kovacs 1993). A meter rule should not be used for this purpose (it often is), because the ends of the ice sample may not be parallel to each other. The more difficult measurement is ice core diameter. Again, a ruler should not be used. A pie tape (Kovacs 1993) or a caliper with long, wide tongs is generally satisfactory, provided the core is ridge-free and of uniform diameter. Where this is not the case, the diameter measured will not be accurate and the volume determination will be off. This is illustrated in Figure 1, which gives a comparison between brine volume determinations made on ~10-cm-long sections from several first-year Arctic sea-ice cores using the equations of Cox and Weeks and Frankenstein and Garner. The regression curve through the data in Figure 1 did not include the outlier (+). The outlier indicates where a measurement error occurred, perhaps because of a volume measurement error.

It is recommended that when the Cox and Weeks (1983) equations are used, and they must be for determining gas volume, total porosity, and

$$v_{B\,(C\text{-}W)} = -1.270 + 1.026\, v_{B\,(F\text{-}G)}$$
$$r^2 = 1.000$$
$$S\,D = 1.15$$
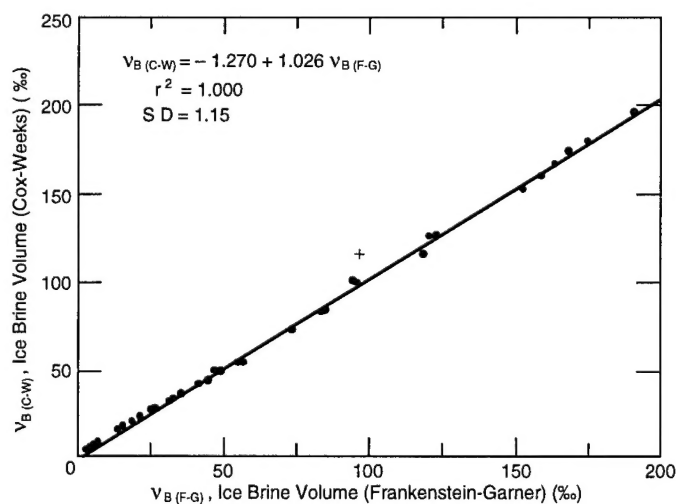
Figure 1. Comparison between the Cox and Weeks and the Frankenstein and Garner methods for calculating sea-ice brine volume. The data point represented by + is considered an outlier.
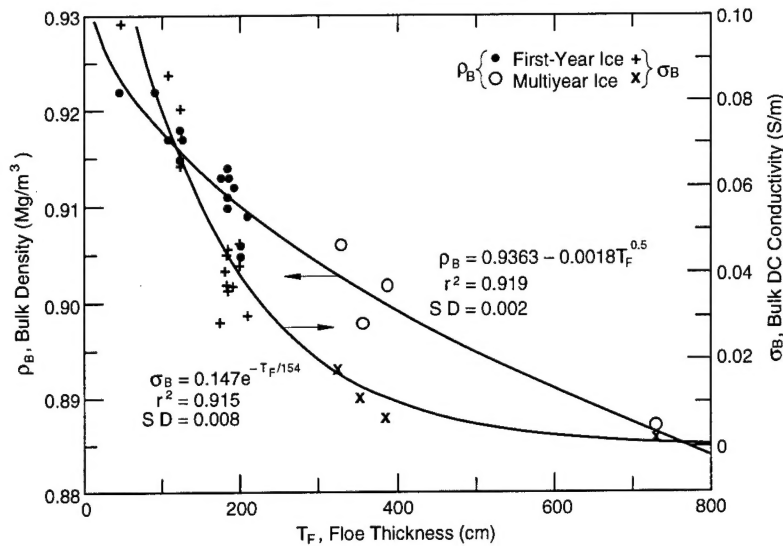
Figure 2. Sea-ice bulk density and conductivity vs. floe thickness.

Figure 2 annotations:
$$\rho_B \begin{cases} \bullet \text{ First-Year Ice } + \\ \circ \text{ Multiyear Ice } \times \end{cases} \sigma_B$$

$$\rho_B = 0.9363 - 0.0018 T_F^{0.5}$$
$$r^2 = 0.919$$
$$S\,D = 0.002$$

$$\sigma_B = 0.147 e^{-T_F/154}$$
$$r^2 = 0.915$$
$$S\,D = 0.008$$

brine-free ice density, the Frankenstein and Garner (1967) equation also be used to estimate the ice brine volume. When the two brine-volume estimates are off by more than 2‰, a measurement or data logging error has occurred. If the problem cannot be resolved, the ice property values calculated with the Cox and Weeks equations should not be used. It should be noted that the Frankenstein and Garner equations for determining brine volume *are not* valid below −23°C. Only the Cox and Weeks equations should be used below this temperature.

The physical and electromagnetic properties of 21 winter Beaufort Sea ice cores, obtained by the author on various field programs, were determined for each 10-cm increment of ice core. Physical property calculations were made using the mathematical expressions of Cox and Weeks (1983). The electromagnetic properties of the ice were determined using the procedures of Kovacs et al. (1987) as modified by Kovacs and Morey (1987). Examples of the calculations are given in Tables 1 and 2. Also assembled were the authors' data from an additional 23 Beaufort Sea ice cores, where only the salinity and temperature of the winter ice were determined for each 10-cm increment of core. For these data, only the brine volume of the ice could be calculated using the equations of Frankenstein and Garner (1967).

From the above data, a number of winter ice floe property trends can be seen. Ice floe bulk density vs. thickness is shown in Figure 2. The bulk density is seen to decrease with ice floe thickness. For the first-year sea ice, the decrease is associated with brine drainage and growth rate

processes, which reduce the volume fraction of the heavier brine entrained within the ice (Kovacs 1996). The lower multiyear ice densities are the result of this ice containing proportionally less brine and more gas, especially in the freeboard portion, which is for all intents and purposes low-density fresh ice. While density is the property that a material's strength is often related to, as with the strength of snow (Kovacs et al. 1969), it is not used for this purpose in sea-ice mechanics. Traditionally, sea-ice failure strength, elastic modulus, and such have been referenced to the brine volume of the ice. This brine volume referencing is still the norm for sea-ice tensile or flexural strength test presentations. The reasoning is that the strength of a material is a function of its solidity. Therefore, the more brine volume there is, the less solid the ice, and the weaker it will be. This method, of course, does not take into account the added porosity associated with the small gas inclusions. Since brine volume, salinity, and temperature are interrelated, brine volume needs to be correlated with these two parameters, as shown in Figure 3. This figure clearly illustrates that, at any given bulk salinity S_B, the bulk brine volume v_B of an ice sheet is dependent on the average ice sheet temperature T_A. While this presentation is enlightening, it does not serve the user very well. More useful is the presentation in Figure 4, where the relationship provided allows for the determination of the bulk brine volume

Figure 3. Sea-ice bulk brine volume vs. bulk salinity with average ice floe temperature as a parameter.

2

Table 1. Physical and electromagnetic properties of 1.23-m-thick sea ice at 100 MHz.*

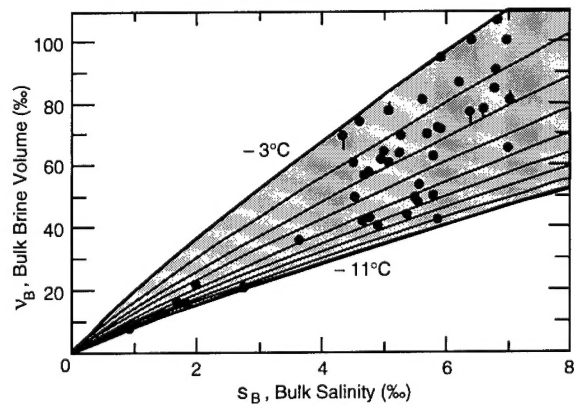| Depth (m)	Core length (cm)	Core diam. (cm)	Core weight (gr)	Melt cond. (mS/m)	Ice temp (-C°)	Bulk den. (Mg/m³)	Ice den. (Mg/m³)	Ice sal. (‰)	Brine vol C-W (‰)	Brine vol F-G (‰)	Air vol. (‰)	Total porosity (‰)	Brine cond. σ_b	Brine diel. ε'_b	Brine diel. ε''_b	Loss tang. ϕ_b	Ice cond. DC σ_{DC}	Ice cond. 100 MHz σ_i	Ice diel. ε_m	Ice diel. ε'_m	Ice diel. ε''_m	Attn (dB/m)	Loss tang. ϕ_i	Phase vel. (m/ns)
0.05	9.80	7.85	431.3	18.05	-7.6	0.909	0.830	10.63	72.3	74.1	23.26	95.6	6.57	59.14	1181.03	19.970	0.086	0.086	10.78	5.15	0.059	43.14	3.025	0.091
0.15	9.79	7.85	432.9	16.23	-7.3	0.914	0.840	9.47	66.9	68.4	17.24	84.2	6.48	59.81	1164.62	19.473	0.075	0.075	9.74	5.04	0.057	39.39	2.679	0.096
0.25	9.83	7.85	437.0	15.31	-6.8	0.919	0.846	8.89	67.1	68.3	11.46	78.5	6.30	60.97	1133.42	18.590	0.073	0.073	9.61	5.07	0.059	38.71	2.601	0.097
0.35	9.73	7.85	432.0	13.43	-6.4	0.917	0.851	7.71	61.2	62.5	11.30	72.5	6.14	61.95	1104.79	17.834	0.061	0.061	8.50	4.90	0.055	34.50	2.257	0.103
0.45	9.78	7.85	431.7	12.93	-5.9	0.912	0.844	7.40	62.7	64.5	16.92	79.6	5.92	63.24	1064.09	16.827	0.062	0.062	8.53	4.92	0.058	34.53	2.254	0.103
0.55	9.81	7.85	437.2	11.92	-4.9	0.921	0.848	6.77	68.4	69.8	7.33	75.7	5.36	66.06	964.68	14.603	0.064	0.065	8.92	5.13	0.071	35.40	2.267	0.100
0.65	9.83	7.85	436.3	11.63	-4.2	0.917	0.836	6.60	76.5	78.3	11.94	88.4	4.89	68.26	879.21	12.880	0.070	0.071	9.59	5.34	0.086	37.45	2.387	0.097
0.75	9.79	7.85	435.5	8.80	-3.4	0.919	0.846	4.89	69.5	70.5	7.71	77.2	4.24	71.05	763.50	10.746	0.052	0.053	7.97	5.15	0.090	30.50	1.838	0.106
0.85	9.78	7.85	434.8	9.21	-2.9	0.919	0.830	5.13	85.3	86.0	9.86	95.1	3.78	72.95	680.46	9.327	0.065	0.066	9.36	5.60	0.124	35.22	2.114	0.098
0.95	9.80	7.85	436.0	10.60	-2.4	0.919	0.795	5.97	120.3	119.7	12.93	133.2	3.27	75.00	588.46	7.846	0.099	0.100	12.93	6.61	0.202	45.71	2.734	0.083
1.05	9.76	7.85	438.2	12.30	-1.9	0.928	0.740	7.01	182.2	177.9	10.20	192.4	2.70	77.22	486.87	6.305	0.163	0.165	19.69	8.49	0.376	60.86	3.499	0.068
Avg	9.79	7.85	434.8	12.76	-4.9	0.918	0.828	7.31	84.8	85.4	12.74	97.5	5.06	66.88	910.10	14.037	0.079	0.080	10.51	5.58	0.112	39.58	2.514	0.095

C-W = Cox and Weeks (1983) equations
F-G = Frankenstein and Garner (1967) equations
σ_b, σ_{DC} and σ_i = S/m

* In the electromagnetic equations (Kovacs and Morey 1987), parameters n and m were 0.1 and 1.65, respectively.

Table 2. Physical and electromagnetic properties of 1.93-m-thick sea ice at 100 MHz.*

Depth (m)	Core length (cm)	Core diam. (cm)	Core weight (gr)	Melt cond. (mS/m)	Ice temp (-C°)	Bulk den. (Mg/m³)	Ice den. (Mg/m³)	Ice sal. (‰)	Brine vol C-W (‰)	Brine vol F-G (‰)	Air vol. (‰)	Total porosity (‰)	Brine cond. σ_b	Brine diel. ε'_b	Brine diel. ε''_b	Loss tang. ϕ_b	Ice cond. DC σ_{DC}	Ice cond. 100 MHz σ_i	Ice diel. ε_m	Ice diel. ε'_m	Ice diel. ε''_m	Attn (dB/m)	Loss tang. ϕ_i	Phase vel. (m/ns)
0.05	9.80	7.85	422.6	10.10	-4.7	0.891	0.830	5.67	57.5	60.6	37.90	95.4	5.24	66.67	941.67	14.125	0.047	0.047	7.19	4.65	0.057	28.92	1.832	0.112
0.15	9.79	7.85	423.9	11.97	-5.3	0.895	0.828	6.81	62.2	65.3	35.24	97.4	5.60	64.89	1007.48	15.526	0.057	0.058	8.13	4.82	0.059	33.07	2.150	0.105
0.25	9.82	7.85	428.2	10.92	-5.5	0.901	0.842	6.16	54.9	57.2	27.29	82.2	5.71	64.32	1027.33	15.971	0.048	0.048	7.22	4.65	0.051	29.13	1.851	0.112
0.35	9.84	7.85	428.7	10.22	-5.5	0.900	0.845	5.74	51.1	53.2	27.49	78.5	5.71	64.32	1027.33	15.971	0.042	0.042	6.72	4.54	0.048	26.81	1.683	0.116
0.45	9.75	7.85	425.5	10.97	-5.4	0.902	0.841	6.19	56.1	58.4	26.60	82.7	5.66	64.60	1017.53	15.570	0.049	0.049	7.35	4.69	0.053	29.65	1.886	0.111
0.55	9.72	7.85	424.5	10.26	-5.2	0.902	0.844	5.76	54.0	56.2	25.37	79.4	5.54	65.18	997.17	15.300	0.045	0.045	7.01	4.63	0.052	27.99	1.758	0.113
0.65	9.77	7.85	426.3	9.06	-4.9	0.902	0.848	5.04	49.8	51.9	25.31	75.1	5.36	66.06	964.68	14.603	0.038	0.038	6.38	4.51	0.050	24.84	1.529	0.119
0.75	9.84	7.85	430.1	8.30	-4.7	0.903	0.853	4.59	47.2	49.1	23.02	70.2	5.24	66.67	941.67	14.125	0.034	0.034	6.03	4.44	0.048	22.83	1.386	0.122
0.85	9.85	7.85	429.7	7.92	-4.4	0.901	0.851	4.36	47.6	49.6	24.76	72.4	5.03	67.61	905.06	13.386	0.033	0.033	5.97	4.45	0.051	22.38	1.351	0.123
0.95	9.76	7.85	430.4	7.61	-4.0	0.911	0.858	4.18	50.4	51.9	14.19	64.6	4.74	68.93	852.16	12.363	0.034	0.035	6.15	4.57	0.058	22.83	1.362	0.121
1.05	9.80	7.85	432.3	7.99	-3.7	0.911	0.851	4.40	57.2	58.7	14.63	71.9	4.50	69.97	809.27	11.567	0.040	0.040	6.74	4.77	0.069	25.53	1.530	0.116
1.15	9.71	7.85	428.3	8.21	-3.5	0.911	0.846	4.53	62.2	63.7	15.21	77.4	4.33	70.68	779.08	11.022	0.044	0.045	7.17	4.91	0.078	27.33	1.640	0.112
1.25	9.81	7.85	432.7	8.46	-3.2	0.911	0.838	4.68	70.1	71.5	16.03	86.1	4.06	71.79	731.32	10.187	0.051	0.051	7.84	5.13	0.093	29.89	1.794	0.107
1.35	9.66	7.85	425.3	8.25	-3.0	0.910	0.834	4.56	72.5	74.0	17.97	90.5	3.88	72.56	687.76	9.616	0.051	0.052	7.93	5.19	0.101	30.05	1.792	0.107
1.45	9.78	7.85	431.0	7.69	-2.8	0.911	0.836	4.23	72.1	73.2	16.71	88.9	3.68	73.35	662.79	9.036	0.048	0.049	7.69	5.18	0.106	28.75	1.691	0.108
1.55	9.87	7.85	435.2	7.20	-2.5	0.911	0.833	3.94	75.4	76.0	16.23	91.7	3.38	74.58	607.61	8.147	0.047	0.048	7.72	5.28	0.120	28.37	1.642	0.108
1.65	9.84	7.85	432.5	6.87	-2.3	0.908	0.828	3.75	77.9	78.3	19.44	97.4	3.16	75.43	568.93	7.542	0.047	0.048	7.72	5.33	0.131	28.07	1.608	0.108
1.75	9.43	7.85	415.9	8.72	-2.0	0.911	0.791	4.84	116.9	116.1	20.41	137.3	2.82	76.76	507.98	6.618	0.082	0.083	11.37	6.45	0.221	40.30	2.315	0.089
Avg	9.77	7.85	428.0	8.93	-4.0	0.905	0.839	4.97	63.1	64.7	22.43	85.5	4.65	69.13	835.94	12.270	0.047	00.047	7.35	4.90	0.080	28.15	1.711	0.112

C-W = Cox and Weeks (1983) equations
F-G = Frankenstein and Garner (1967) equations
σ_b, σ_{DC} and σ_i = S/m

* In the electromagnetic equations (Kovacs and Morey 1987), parameters n and m were 0.1 and 1.65, respectively.

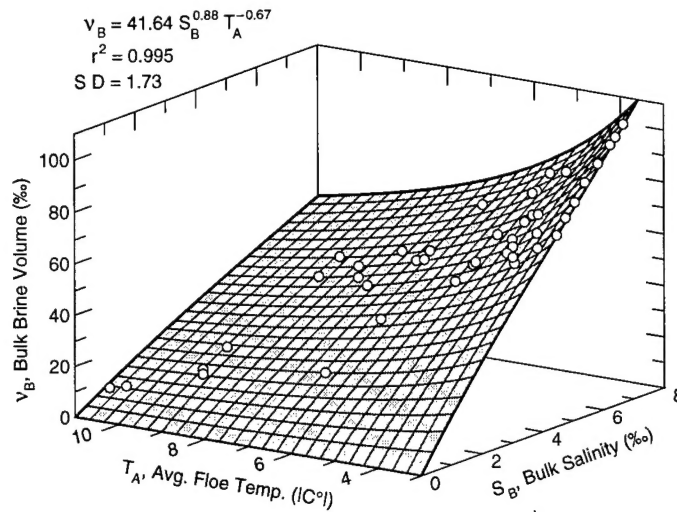$$v_B = 41.64\, S_B^{0.88}\, T_A^{-0.67}$$
$$r^2 = 0.995$$
$$SD = 1.73$$

Figure 4. Sea-ice bulk brine volume vs. average absolute ice temperature and bulk salinity.

vs. ice-sheet average temperature and bulk salinity. It should be realized that Figure 3 is an end view of the 3-D data presentation in Figure 4. In Figure 3, the points with no vertical tails are within one standard deviation (SD) of the brine volume surface shown in Figure 4. Points with tails lie between one and two standard deviations of the brine volume surface, which is located at the tip of the vertical line.

TENSILE AND FLEXURAL STRENGTH

The equation for predicting the bulk brine volume v_B in ‰ as a function of S_B and the absolute value of T_A (Fig. 4),

$$v_B = 41.64\ S_B^{0.88}\ T_A^{-0.67}, \qquad (1)$$

along with the expressions of Kovacs (1996) for estimating the bulk salinity (‰) of first-year sea ice vs. ice floe thickness T_F (cm) (Fig. 5),

$$S_B = 4.606 + 91.603\ /T_F, \qquad (2)$$

offer the opportunity to make other ice property assessments, which in turn can be used to estimate ice sheet strength.

For example, the horizontal uniaxial tensile strength σ_t of an ice sheet could be estimated using the empirical equation of Dykins (1970):

$$\sigma_t = 0.816 - 0.069\ v_B^{0.5}. \qquad (3)$$

Similarly, ice floe flexural strength σ_f may be estimated using the empirical equation (Timco and O'Brien 1994)

$$\sigma_f = 1.76\,e^{-5.88\sqrt{v_B}}. \qquad (4)$$

These expressions could be used as follows. Ice thickness is determined by drill-hole measurement. Then from eq 2 the bulk salinity of the ice is estimated. Ice temperature is determined next at 20–25 cm below the ice surface. A linear temperature gradient to the ice/water interface (~1.7°C) is assumed, and the average ice sheet temperature is calculated. The bulk salinity and average temperature values are then used in eq 1 to determine the bulk brine volume. This value can now be used in eq 3 or 4 to determine σ_t or σ_f, respectively. It should be noted that Gavrilo et al. (1995) compared various published expressions for determining the flexural strength of sea ice and found that eq 4 gave σ_f values 2 to 4 times higher than other research results. Further evaluation of the various σ_f equations may be in order.

The above procedure still requires a drill-hole thickness and a near-surface ice temperature measurement. These measurements may not be necessary. Using the formulations for determining the electromagnetic properties of sea ice (Kovacs and Morey 1987), the low-frequency (DC to ~100 MHz) bulk conductivity* σ_B of a model sea-ice

---

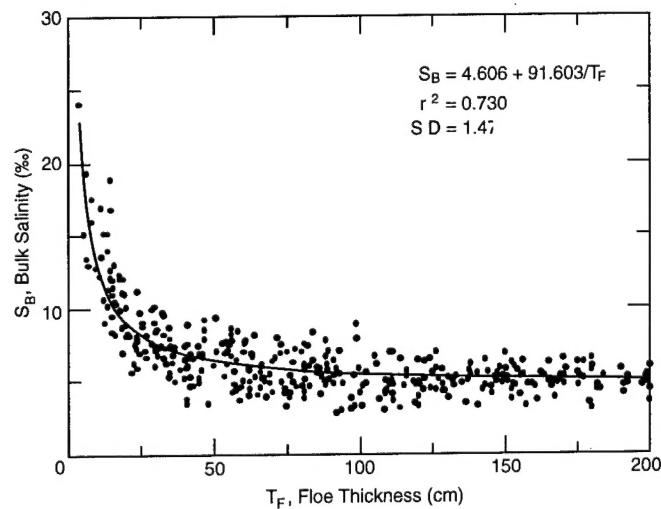* Sea-ice conductivity is approximately constant between DC and 100 MHz (see Tables 1 and 2).

$$S_B = 4.606 + 91.603/T_F$$
$$r^2 = 0.730$$
$$SD = 1.47$$

Figure 5. Combined Arctic and Antarctic ice floe bulk salinity vs. thickness (from Kovacs 1996).

$$v_B = 9.02 + 217.09/T^2 + 528.48\sigma_B$$
$$r^2 = 0.996$$
$$S\,D = 0.98$$

Salinity = 7‰

4‰

v_B, Brine Volume (‰)

σ_B, Bulk DC Conductivity (S/m)

T, Temperature (°C)

Salinity = 7‰

4‰

v_B, Brine Volume (‰)

σ_B, Bulk DC Conductivity (S/m)

T, Temperature (°C)

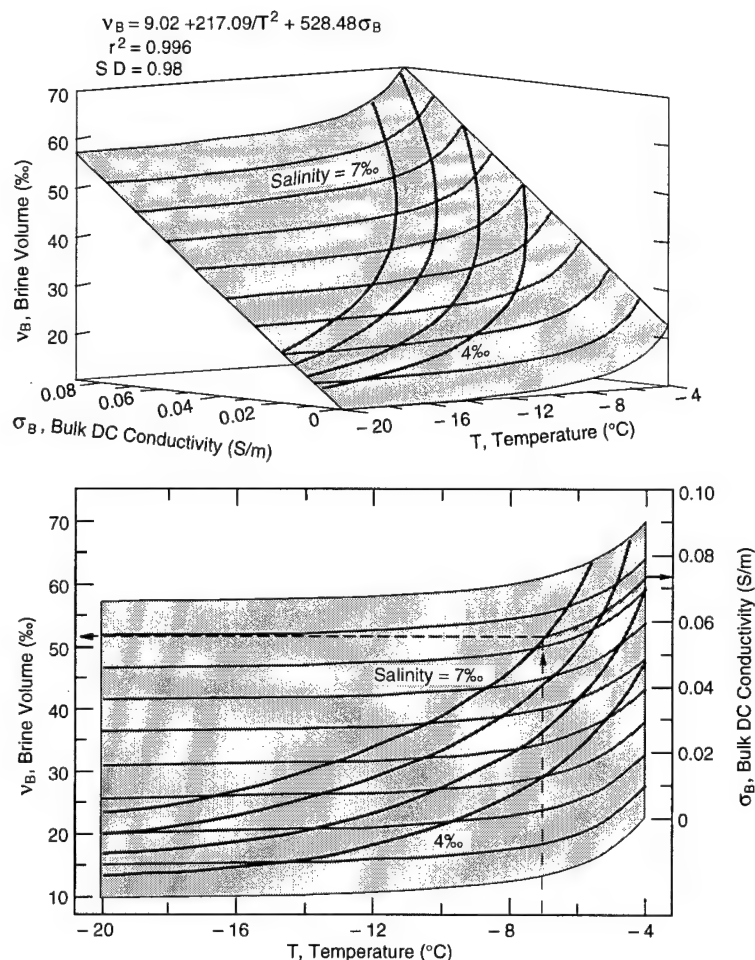*Figure 6. 3-D presentation of sea-ice brine volume vs. DC conductivity and temperature with salinity as a parameter for an ice density of 0.911 Mg/m³ (a) and a boresight view from the above temperature window (b).*

increasing ice floe thickness as revealed in Figure 2 affects all other ice properties. It turns out that this effect is favorable to the remote sounding of sea ice. For example, Kovacs and Morey (1991) and Kovacs et al. (1996) have shown that a portable electromagnetic induction sounding system can be used to measure remotely an apparent bulk conductivity from which an estimate of winter Beaufort Sea ice thickness can be made (Fig. 7). When the v_B vs. σ_B at DC values listed in Tables 1 and 2 and from 20 other ice floes were compared, it was found that the calculated bulk conductivity of Beaufort Sea ice was directly related to v_B, as shown in Figure 8. Therefore, in principle, it should be possible to estimate both undeformed winter Arctic ice floe thickness and bulk brine volume remotely using a conductivity measurement system. Before the latter is possible, the relation between the field- measured apparent bulk conductivity, which is highly affected by the underlying seawater, and the bulk brine volume of sea ice floes of various thicknesses will need to be determined. Conductivity measurement at a frequency well above 50 kHz is likely to be necessary to separate the sea-ice conductivity con-

sheet was determined along with its brine volume v_B vs. ice temperature and salinity. An ice sheet bulk density of 0.911 Mg/m³ was used in the determinations. The calculated results are graphically shown in Figure 6. There is a decrease in brine volume with decreasing ice temperature. In addition to ice conductivity, Figure 6 indicates that either ice salinity or temperature is required to estimate v_B.

The complex interrelationship between the model sea-ice temperature, salinity, brine volume, and conductivity is well revealed in Figure 6. The results suggest that determining σ_B of natural sea ice remotely will not, of itself, allow v_B to be estimated. Not revealed is the effect of density, which was fixed at 0.911 Mg/m³ for this example. The decrease in the bulk density and conductivity with

Instrument Conductivity Reading (S/m)

Drill-hole-Measured Snow and Ice Thickness (m)

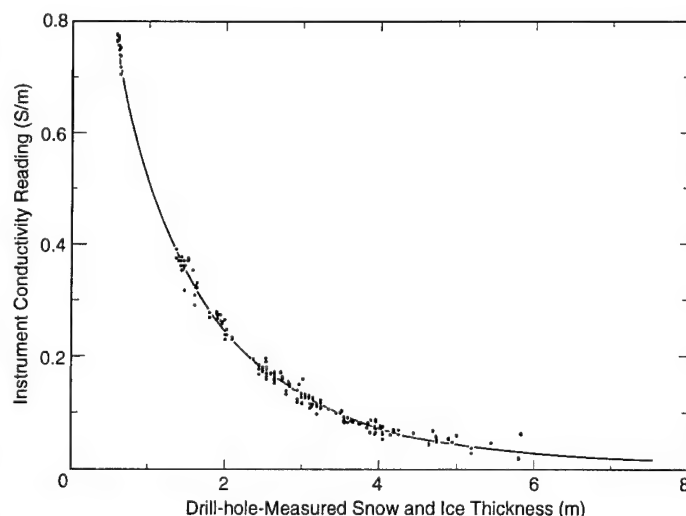*Figure 7. EM-31 instrument conductivity reading at ~10 kHz vs. ice floe snow plus ice thickness (from Kovacs et al. 1996).*
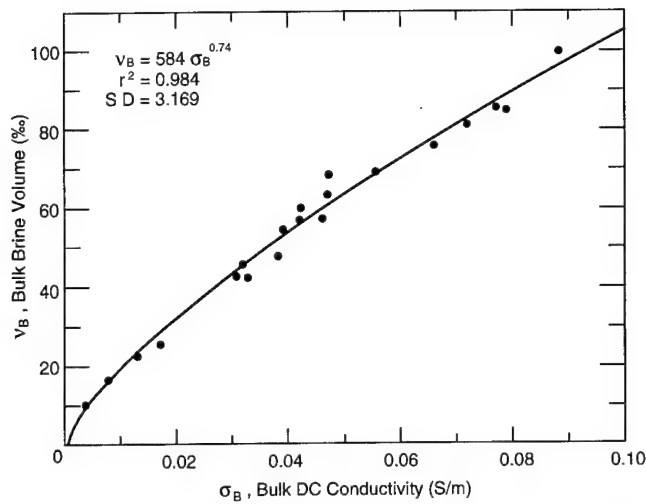
5

Figure 8. Measured sea-ice floe bulk brine volume vs. the calculated bulk DC conductivity of the ice.
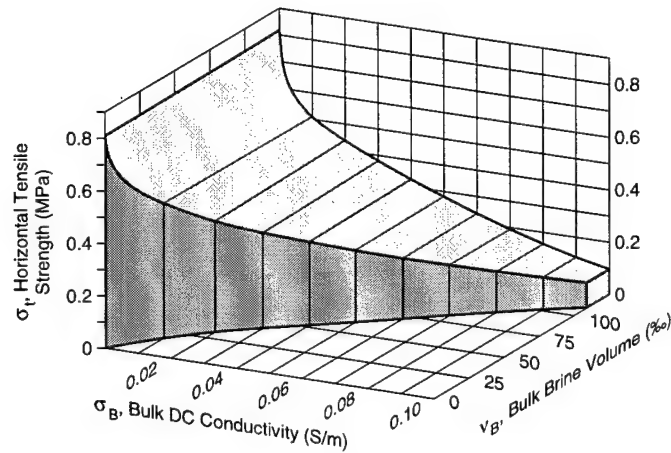

Figure 9. Ice sheet horizontal tensile strength vs. bulk DC conductivity and brine volume.
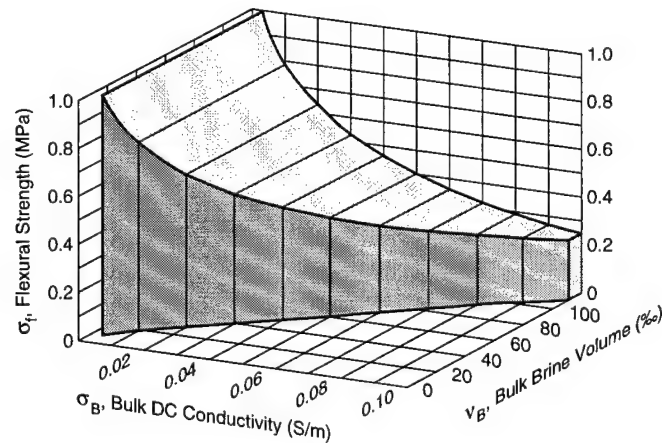

Figure 10. Ice sheet flexural strength vs. bulk DC conductivity and brine volume.

tribution from the seawater conductivity contribution. A dual high and low frequency system or a wideband measurement system could be used.

In the interim, an off-the-shelf electromagnetic induction system operating at 10 kHz can be used to estimate ice thickness (Fig. 8), and the bulk salinity of the ice is estimated using eq 2. After determining the average ice sheet temperature, as previously described, eq 1 can be used to calculate the bulk brine volume. Ice strength may then be calculated from eq 3 or 4.

The relation between sea-ice tensile or flexural strength, brine volume, and the calculated bulk DC conductivity of natural sea ice is shown in Figures 9 and 10. These figures are the result of using the equation in Figure 6 and eq 3 and 4, respectively. In the future, using similar equations, an algorithm could be added to a portable electromagnetic induction sounding system that would provide both ice thickness and strength from the apparent sea-ice conductivity measurements.

COMPRESSIVE STRENGTH

Estimating the compressive strength of sea ice is different. While the uniaxial tensile or flexural strength of sea ice does not reveal a significant strain rate dependence, at the strain rates of interest for most ice engineering problems, the compressive strength does. In addition, in reporting sea-ice compression test results, the recent, and correct, method is to relate strength to total porosity: brine volume plus gas volume. Recently, Timco and Frederking (1990) developed empirical equations for predicting the large-scale uniaxial unconfined compressive strength of Arctic sea ice. Their equations are based on small-scale strength tests and the various controlling factors, such as ice structure, brine volume, porosity, loading direction (horizontal–vertical), and strain rate. Their strength equation for horizontally loaded columnar sea ice is

$$\sigma_c = 37\,\dot{\varepsilon}^{0.22}\left[1-\left(\phi_B / 270\right)^{0.5}\right], \quad (5)$$

6

Table 3. Field-measured and calculated test data.

Ice thick.[a] cm	Avg temp.[a] −°C	Bulk salinity ‰		Bulk brine volume ‰		Bulk porosity ‰		Strain rate[a] s⁻¹	Measured[a] MPa	Calculated MPa			
156	10.6	5.50[1]	5.20[2]	38.19	36.53[3]	52.87	51.18[4]	7.90e−7	0.81	0.96[5]	0.38[6]	0.51[7]	0.54[8]
154	10.5	5.54	5.20	38.44	36.26	53.10	51.39	1.10e−6	0.49	1.03	0.46	0.57	0.60
120	12.9	6.08	5.37	34.18	32.94	49.20	47.97	1.27e−6	0.66	1.07	0.52	0.62	0.67
129	10.7	5.94	5.32	38.50	32.04	53.16	51.64	9.20e−6	1.00	1.62	1.12	1.10	1.17
152	10.5	5.57	5.21	38.50	36.82	53.16	51.94	1.42e−5	1.30	1.81	1.30	1.26	1.35
166	4.2	5.34	5.16	70.67	67.46	82.66	79.20	9.00e−5	1.82	2.15	1.86	1.79	1.60
147	5.9	5.65	5.23	56.83	54.36	69.96	67.28	9.10e−5	1.86	2.36	2.04	1.95	1.88
154	4.3	5.54	5.20	69.91	66.86	81.96	78.65	1.33e−4	2.10	2.33	2.09	2.03	1.83
146	11.8	5.66	5.24	35.72	34.23	50.61	49.12	1.56e−4	2.86	3.11	2.70	2.71	3.00
130	5.1	5.92	5.32	63.26	60.85	75.86	73.18	2.16e−4	1.88	2.66	2.50	2.45	2.28
161	7.3	5.42	5.18	48.89	46.74	62.67	60.37	3.40e−4	3.53	3.41	3.08	3.08	3.17
129	3.4	5.94	5.32	83.08	79.84	93.96	90.54	7.50e−4	2.62	2.86	3.13	3.24	2.77

a = EXXON Test Data
1 = Timco & Frederking eq 6 or 7
2 = Eq 2
3 = Eq 1
4 = Figure 13's equation

5 = Timco & Frederking, eq 5
6 = Timco & Frederking, revised, eq 8
7 = Figure 18's equation
8 = Eq 10

where σ_c = horizontal uniaxial unconfined compressive strength (MPa)

$\dot{\varepsilon}$ = strain rate, s⁻¹

ϕ_B = bulk ice porosity (‰).

Timco and Frederking compared σ_c values determined from eq 5 with in-situ, full ice sheet thickness, horizontal, uniaxial unconfined compression tests performed by Exxon on Beaufort Sea ice. The Exxon large-scale test data comprised ice thickness, average ice temperature, loading strain rate, and the measured strength (Table 3). Since the bulk porosity of the ice sheets tested was not provided, the authors had to make these estimates. To do this, they first included additional data in Figure 11 and, following the same approach as Cox and Weeks (1974), ran two linear regression curves through the data. Only slightly different from the Cox and Weeks equations (Fig. 11), the new equations are:

$$S_B = 13.4 - 0.174\,T_F \qquad (6)$$

for $T_F \le 0.34$ cm; and

$$S_B = 8.0 - 0.016\,T_F \qquad (7)$$

for $T_F > 0.34$ cm.

From these equations, Timco and Frederking determined S_B for each ice sheet tested (Table 3). Then the bulk density of the sea ice was selected to be 0.907 Mg/m³. With these determinations and the average ice floe temperature given in Table 3, the expressions provided by Cox and Weeks (1983) were used to calculate the bulk porosity of each ice sheet. Note that these values were not provided by Timco and Frederking in their paper. The missing bulk porosity values were recalculated along with the bulk brine volume for each ice sheet. The values are listed in the left column of the brine volume and porosity data columns in Table 3. The σ_c strengths measured by Exxon and calculated by Timco and Frederking are compared in Table 3 and shown graphically in Figure 12. The regression curve in Figure 13 shows that the calculated values are generally higher than the measured ones. This offset may be due to small- to large-scale scaling ambiguities.

To bring eq 5 into better agreement with the Exxon test results, the bulk salinity and brine volume of each ice sheet were determined using eq 2 and 1, respectively. Next, the S_B, T_A, and ϕ_B data from Tables 1 and 2 and others referenced were plotted as shown in Figure 13a. A boresight view of the data as seen looking into the salinity "window" is shown in Figure 13b. This view clearly
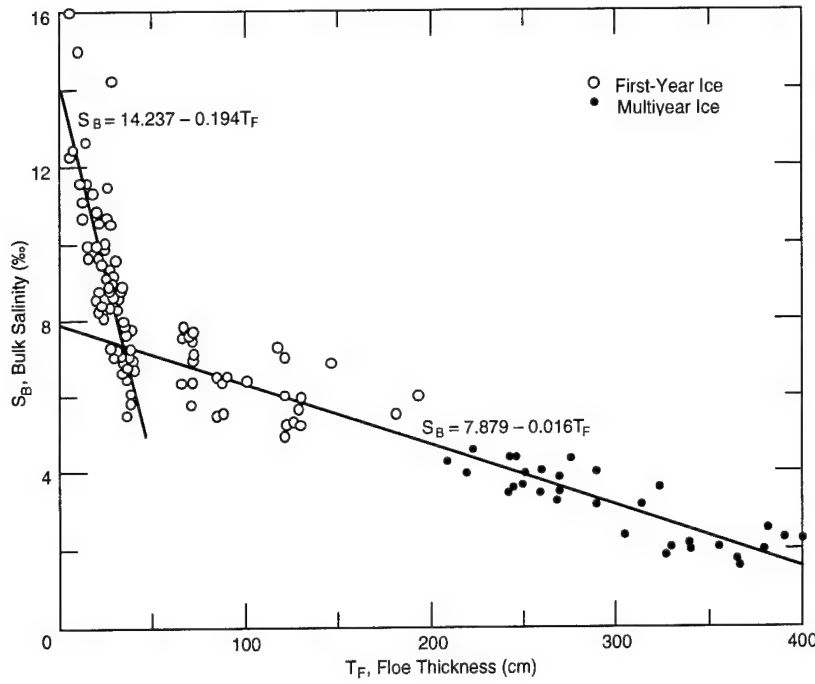
Figure 11. Sea-ice bulk salinity vs. floe thickness (after Cox and Weeks 1974).
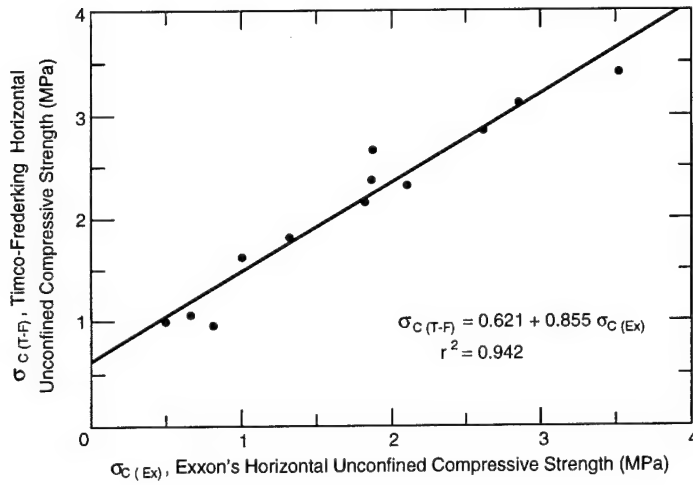

Figure 12. Timco and Frederking estimated full ice sheet horizontal unconfined compressive strength vs. Exxon's field-measured values.

reveals the interrelationship of average ice sheet temperature and bulk salinity with the bulk porosity.

Using the S_B values determined from eq 2, the average ice floe temperature listed in Table 3, and the equation provided in Figure 13, ϕ_B was estimated for each of the Exxon ice sheets. These v_B, S_B, and ϕ_B values are listed in Table 3 as the right column under each respective heading. Using the new ϕ_B values and the related strain rates in Table 3, σ_c was recalculated using eq 5. These so-called modified σ_c values were then compared (Fig. 14) with the σ_c estimates made by Timco and Frederking (Table 3). As can be seen in Figure 14, using the above ϕ_B estimates in eq 5 gives σ_c values that are comparable with those of Timco

and Frederking. However, the modified method for determining σ_c gives values that are still offset from the Exxon field test results (Fig. 15). To alleviate this offset, eq 5 was revised to read

$$\sigma_c = 37\,\dot{\varepsilon}^{0.22}\left[1-\left(\phi_B^{0.93}/270\right)^{0.5}\right]-0.65. \qquad (8)$$

This revision brings the σ_c values (Table 3) into better agreement with the field determinations, as shown in Figure 16.

If the DC conductivity of the ice could be determined remotely along with ice sheet thickness, then S_B could be determined from eq 2 and v_B estimated from an expression similar to that given in Figure 6 and ϕ_B from Figure 17. The data in

Figure 17 are from Tables 1 and 2 and the sources cited above. This figure indicates that nonde-formed Beaufort Sea ice floes have a gas volume between about 1 and 2%.

The σ_c values calculated using eq 8 in relation to the controlling parameters $\dot{\varepsilon}$ and ϕ_B can be an-alyzed using a two-parameter power function. The relationship is a further development of the Norton (1929) secondary creep rate equation con-taining a power function of stress:

$$\dot{\varepsilon} = B\sigma^n,$$

where B is an empirical parameter that takes into account ice structure, temperature, activation en-ergy, and other factors, σ is the applied stress, and the empirical exponent n is generally found to be about 3 for ice. Rearranging for σ, the above equa-tion becomes

$$\sigma = B_1 \, \dot{\varepsilon}^{1/n},$$

where $B_1 = B^{-1/n}$. The former expression was used by Glen (1955, 1958) to evaluate the creep behav-ior of solid, not porous, freshwater ice. Since the ice porosity has a profound effect on σ, the above equation must be modified to include a porosity parameter ϕ as follows:

$$\sigma = B_2 \, \dot{\varepsilon}^{1/n} \, \phi^m, \tag{9}$$

where $B_2 = B_1 \phi^{-m}$ and m is an empirical exponent.

Equation 9 was evaluated by substituting the σ_c values obtained from eq 8 for σ in eq 9 and using the related controlling parameters ϕ_B and $\dot{\varepsilon}$ given in Table 3. The result is shown in Figure 18. Equation 9 is shown to statistically fit the data extremely well with an r^2 value of 0.993.

As more data become available, the failure sur-face and therefore the variables in eq 9 may be better determined. Even though the failure sur-face fits the data with a high r^2 value of 0.993, the data suggest that this surface is not a straight line as viewed from the strain rate window in Figure
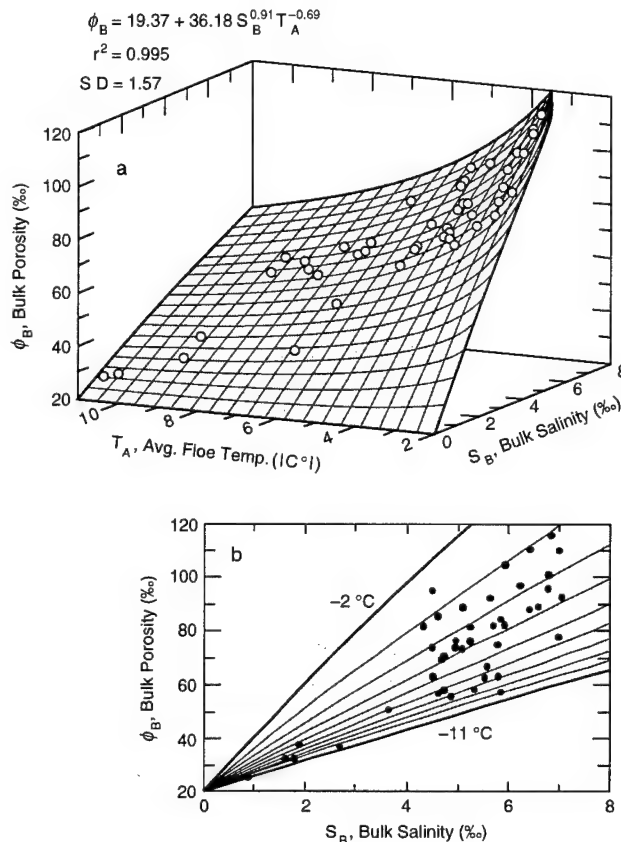

Figure 13. Ice floe bulk porosity vs. average temperature and bulk salinity (a) and boresight view from the above bulk salinity window (b).
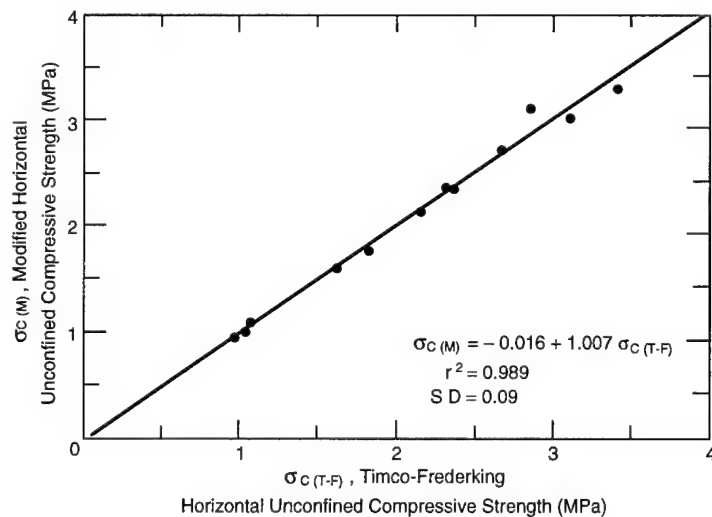

Figure 14. Modified Timco–Frederking ice floe σ_c strengths vs. their original values.

9
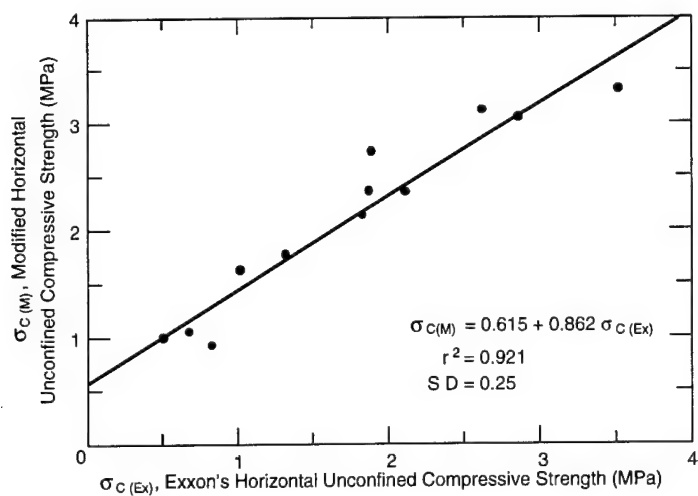
Figure 15. Modified Timco–Frederking ice floe σ_c strengths vs. Exxon's field-measured σ_c values.
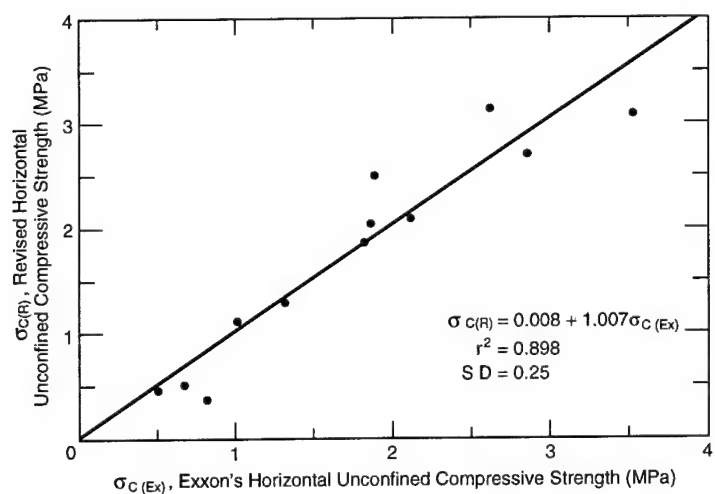

Figure 16. Ice floe σ_c strengths calculated using eq 8 vs. Exxon's field-measured σ_c values.
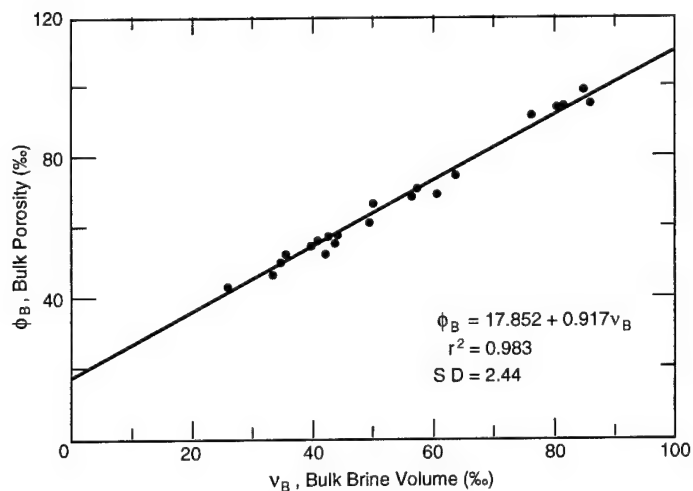

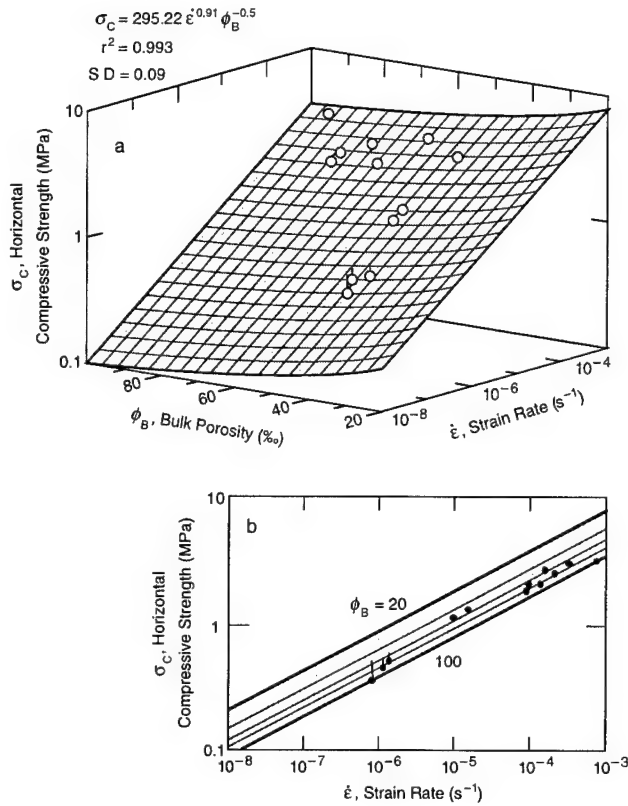*Figure 17. Sea-ice floe bulk porosity vs. bulk brine volume.*

10

Figure 18. Equation-8-determined ice floe σ_c strengths vs. bulk porosity and strain rate (a) and the boresight view from the above strain rate window (b).
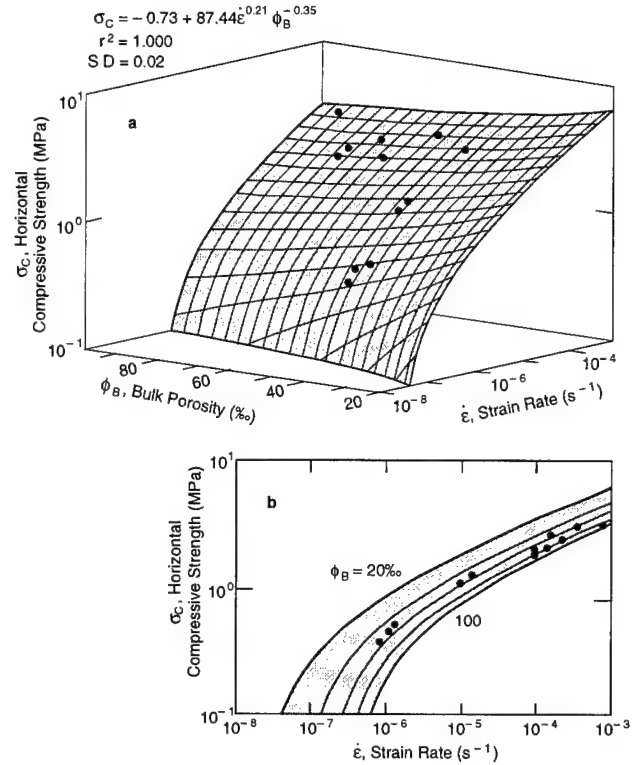
Figure 19. Equation-8-determined ice floe σ_c strengths vs. bulk porosity and strain rate (a) and the boresight view of the above from the strain rate window (b).

18b. The three data points at a strain rate of about 10^{-6} are shown to be offset from their predicted failure surface position at the tip of their vertical tails, suggesting that the failure surface curves downward. This is not surprising if B contains a nonlinear viscosity component. In this case, while stress is still a function of strain rate, it is not directly proportional (Mellor 1986), at least at strain rates between about 10^{-5} and 10^{-3} as indicated by the stress vs. strain rate curves for fresh and saline ice given in Sanderson (1988). The Exxon data fall in the ductile-to-brittle strain rate transition region where the creep power-law may not be valid, that is, $\dot{\varepsilon} \neq B\sigma^n$ because n is no longer a constant.

A statistically more representative failure surface for the data is shown in Figure 19a. This curved surface fits the data with a correlation coefficient of $r^2 = 1.000$. A boresight view of the data from the strain rate window in Figure 19a is shown in Figure 19b. Based on the data presented by Sanderson (1988), be-

low a strain rate of about 10^{-6} the failure surface should be linear, $a \approx 3$. However, the existing data are insufficient for developing this trend. In the interim, for strain rates between 10^{-4} and 10^{-3}, the equation given in Figure 18 is preferred because it does not contain a second constant. The equation for the failure surface when v_B is substituted for ϕ_B in Figure 18 is $\sigma_c = 150.75 \ \dot{\varepsilon}^{0.31} \ v_B^{-0.36}$. In this expression, v_B implicitly accounts for the bulk gas volume or the porosity. In using either σ_c expression, the only parameters needed are the loading strain rate and the bulk ice porosity or brine volume. The latter may one day be estimated from remote conductivity measurements along with ice thickness using a helicopter-borne electromagnetic induction sounding system (Kovacs and Holladay 1990).

A comparison of the σ_c data derived from using eq 8 with the horizontal uniaxial unconfined compressive strength data of others should be of interest. The data compiled by Sanderson (1988; see his Fig. 4.8) are shown in Figure 20 for the strain rate range of our data. In this standard
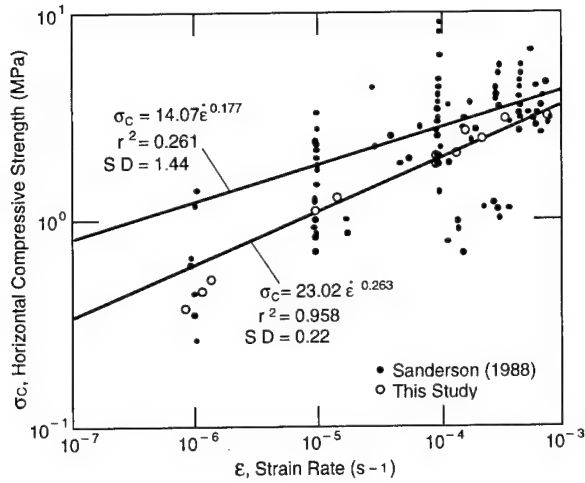
11

Figure 20. Ice floe σ_c values calculated using eq 8 from the study compared with the data provided by Sanderson (1988). The data were fitted with a single-term power equation.
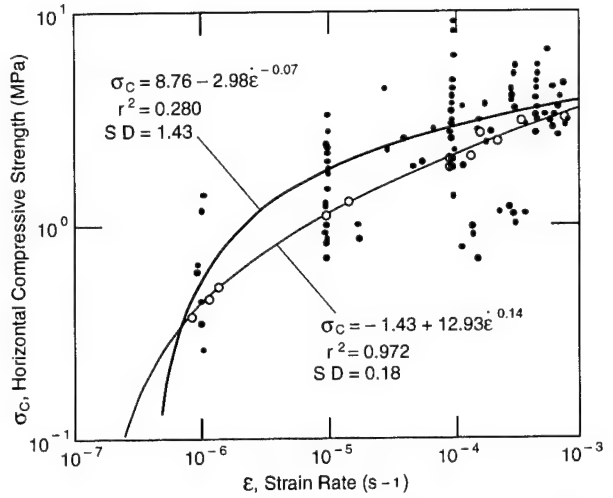

Figure 21. Ice floe σ_c values calculated using eq 8 from this study compared with the data provided by Sanderson (1988). The data were fitted with non-log-log power equations.

presentation, no corrections have been made to the data to account for differences in test technique, ice porosity, grain size, or crystal orientation. This is not unusual since some of these parameters were not measured or provided in the original source material, as is the case for the Exxon data used in this report. For this reason there is considerable scatter in the data. The upper regression curve shown in Figure 20 fits the data from Sanderson; the lower curve represents the data generated from eq 8. The small amount of data from this study coupled with the unknowns mentioned above does not allow a definitive statement to be made on the difference between the two lines. Clearly, the data from this study fit well within the scatter of the data from Sanderson. Both sets of data are statistically better represented by the nonlinear curves shown in Figure 21. Here again, the failure surface appears to be a non-power-law function of the strain rate.

The Timco and Frederking (1990) study, which resulted in the formulation of eq 6, is based on small-scale test results. How applicable this equation is to full-scale ice force assessments can be questioned on the basis of small- to large-scale scaling uncertainties. To avoid this problem, the full-scale Exxon σ_c data were directly analyzed using the values listed in the right-hand bulk porosity column in Table 3. Applying eq 9 to analyze the σ_c and $\dot{\varepsilon}$ data of Exxon vs. the above-related ϕ_B values (Fig. 22a) gives the following expression for the failure surface:

$$\sigma_c = 1970 \, \dot{\varepsilon}^{0.32} \, \phi_B^{-0.95}. \tag{10}$$

In the boresight view of the data from the strain rate window in Figure 22b, the "outlier" with the long offset tail at a strain rate of $7.9 \times 10^{-7} \text{s}^{-1}$ is very apparent. However, removing this data point and reanalyzing the remaining data gives a new equation whose calculated σ_c values do not vary by more than 0.04 MPa from those calculated by eq 10.

The form of the expression for the curved failure surface shown in Figure 17 does not fit the new data set as well as the power type equation in Figure 22. This may be seen by comparing the statistics listed in Figure 22 with those in Figure 23. The boresight view of the failure plane from the strain rate window (Fig. 23b) also indicates no fit improvement for the outlier over the failure surface shown in Figure 22b.

Substituting the new v_B data for the ϕ_B data and reanalyzing as before gives the results shown in Figure 24. The expression for the failure surface is now

$$\sigma_c = 523.24 \, \dot{\varepsilon}^{0.32} v_B^{-0.67}. \tag{11}$$

As with the bulk porosity data, applying a curved failure surface through the σ_c vs. bulk brine volume and $\dot{\varepsilon}$ data does not result in a statistically better curve fit.

It is interesting that the σ_c vs. $\dot{\varepsilon}$ trend, as obtained with eq 8 and from Sanderson's data, ap-

12

Figure 22. Exxon ice floe σ_c values vs. bulk porosity and strain rate (a) and the boresight view of the above from the strain rate window (b). Data were fitted with a two-term power function, i.e., eq 9.
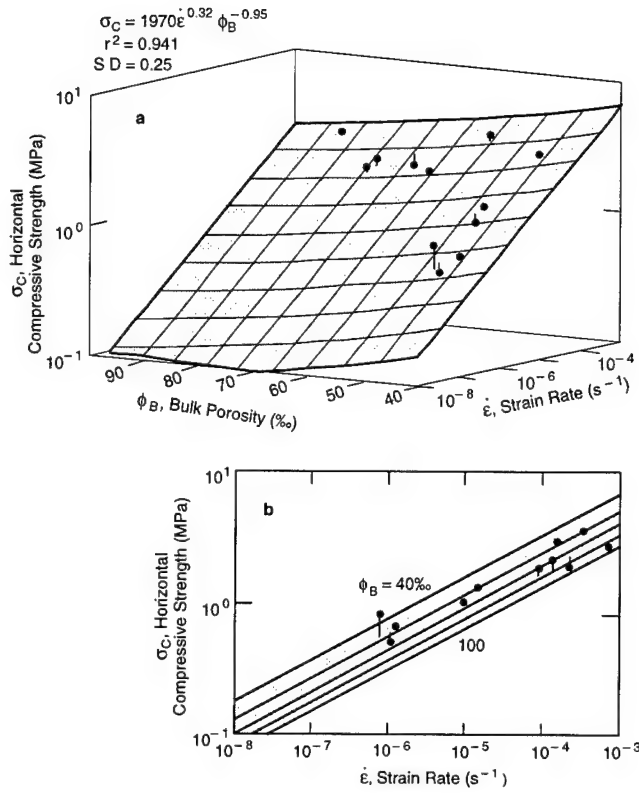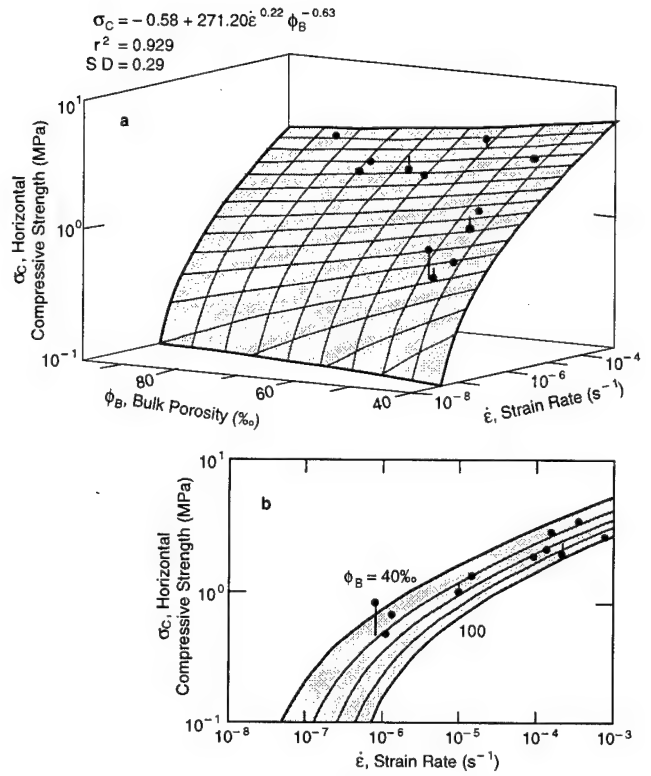

Figure 23. Ice floe σ_c values vs. bulk porosity and strain rate (a) and the boresight view of the above from the strain rate window (b). Data were fitted with a non-log-log power equation.
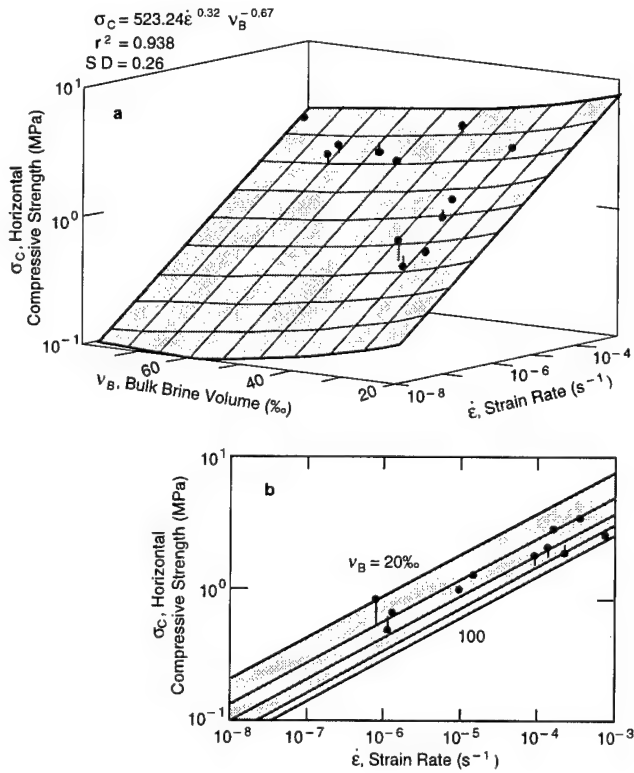

Figure 24. Ice floe σ_c values vs. bulk brine volume and strain rate (a) and the boresight view of the above from the strain rate window (b).
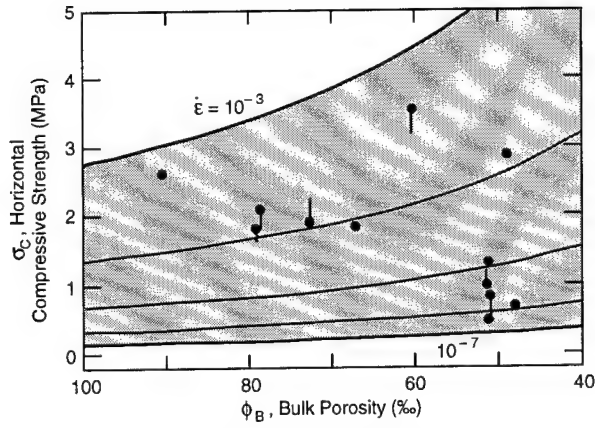
13

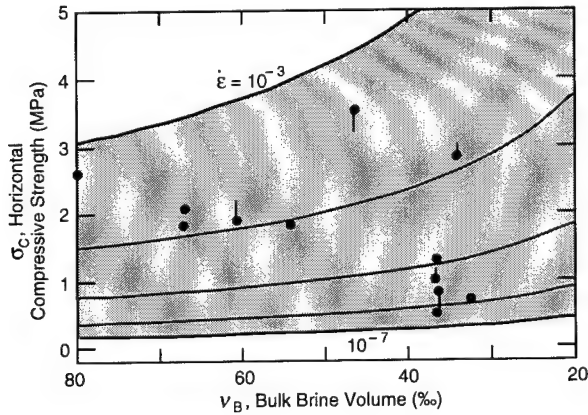*Figure 25. Boresight view from the bulk porosity window in Figure 22a.*

Figure 26. Boresight view from the bulk brine volume window in Figure 24a.

pears to favor a curved failure surface (Fig. 17 and 19), while the trend resulting from the analysis of the Exxon σ_c vs. $\dot{\varepsilon}$ data does not show a strong preference. Additional full ice sheet tests should help to further define the failure surface, especially outside the area of the current data. Within the range of the current data, $10^{-6}s^{-1} < \dot{\varepsilon} < 10^{-3}s^{-1}$ and $\sim25‰ < v_B < 80‰$, eq 11 well represents the σ_c strength of sea ice as determined from full-scale in-situ tests. This is equally true for eq 10 and its counterpart in Figure 23a, in which ϕ_B is a parameter. Nevertheless, eq 10 is preferred because of its simpler form; it does not contain a secondary constant. In addition, outside the range of this field data, the latter equation predicts an unrealistic zero ice strength between strain rates of about 10^{-7} and $10^{-8}s^{-1}$.

The relationship of bulk porosity and strain rate to sea ice strength is clearly revealed in Figure 25. The effect of ϕ_B on σ_c is shown to be signi-

ficantly greater at the higher strain rates. As would be expected, the same trend is maintained when v_B is substituted for ϕ_B (Fig. 26).

If one assumes that n and m are 3 and –1 respectively, then eq 10 can be simplified to

$$\sigma_c = 2.7 \times 10^3 \; \dot{\varepsilon}^{1/3} \; \phi_B^{-1}. \tag{12}$$

σ_c values calculated from eqs 10 and 12 were compared and found to cross-correlate with an $r^2 = 1.000$ and a standard deviation of 0.012 over the range of the Exxon full-scale test data.

By rearranging eq 9, one obtains an equation for the secondary creep of sea ice:

$$\dot{\varepsilon} = B_3 \, \sigma^n \phi^w, \tag{13}$$

where $B_3 = B_2^{-n}$ and $w = -mn$.

To take into account the creep process of ice with time, eq 13 can be modified to describe primary creep as follows:

$$\dot{\varepsilon} = B_4 \, \sigma^n \, \phi_B^w \, t^\lambda, \tag{14}$$

where parameter B_4 will be (and the magnitude of exponents n and m may be) different from those in eq 13, and λ is an exponent.

For a more complete description of the creep process of ice under a complex stress–strain state, the reader is referred to the recent work of Fish (1993).

ICE–STRUCTURE INTERACTION FORCE

As is well recognized by engineers engaged in estimating sea-ice forces on offshore structures, many variables enter into the calculations. In the following, an estimate is made of the horizontal force that could develop between a cold first-year sea-ice sheet and an offshore structure in the southern Beaufort Sea. In this scenario only the structure width (90 m) and the degree-days of seawater freezing since a stable ice cover formed (5000) are known. From the work of Anderson (1961), Wen et al. (1991), and R. Lewellen (pers. comm.), the relationship between Arctic ice floe thickness and the cumulative freezing degree-days since a stable ice cover formed was determined (Fig. 27). This curve in Figure 27 is based on sea-ice field measurements with a natural snow cover. From the equation for the curve in Figure 27, the expected ice thickness for 5000 freezing degree-days is 176 cm, and from eq 2 the bulk salinity of the ice
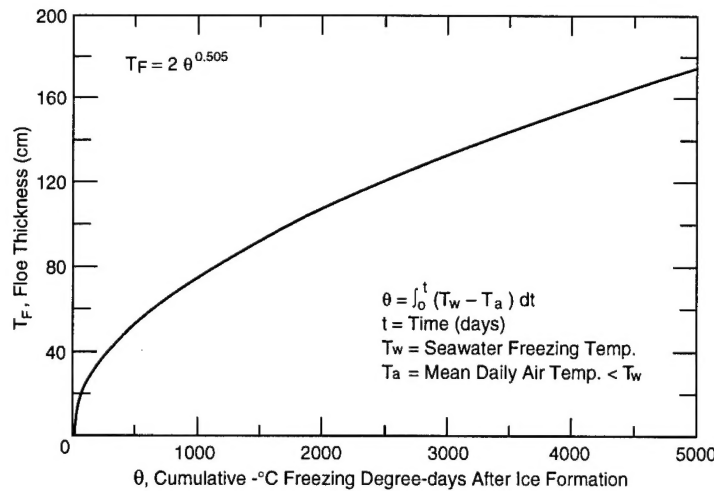
14

Figure 27. Sea-ice thickness vs. seawater freezing degree-days after a stable ice cover has formed.

sheet is estimated to be 5.15‰. We assume the ice sheet has an average temperature of –10°C. This is a reasonable value for cold, late-winter first-year sea ice along the Alaska Beaufort Sea coast. The bulk porosity is found to be 52.20‰ from the equation, $\phi_B = 19.37 + 36.18\ S_B^{0.91}\ T_a^{-0.69}$, given in Figure 13a.

The peak failure stress in sea ice occurs at a strain rate of about $10^{-3}s^{-1}$ for small-scale ice samples with an aspect ratio less than 2. As the sample size or the volume of ice under load increases, the peak stress occurs at a lower strain rate (Sanderson 1988, Gavrilo 1995). At full-scale ice structure interaction when the aspect ratio is greater than 50, the peak stress appears to occur at an effective strain rate $\dot{\varepsilon}_e$ around $10^{-5}\ s^{-1}$. Since the structure width d is very much greater than T_F, plane stress conditions apply and the apparent ice sheet velocity V at this strain rate is (Sanderson 1988)

$$V = \dot{\varepsilon}_e\ 0.44d \qquad (15)$$

or 1.4 m/h. Using 52.2‰ for ϕ_B and $10^{-5}\ s^{-1}$ for $\dot{\varepsilon}$ in eq 5 gives 1.6 MPa for the ice sheet peak horizontal uniaxial unconfined compressive strength. For plane stress conditions, the indentation force F between a vertical structure and the level ice sheet may be estimated using the reference stress expression (Sanderson 1988)

$$F = 1.15\ dT_F\sigma_c. \qquad (16)$$

For d = 90 m, T_F = 1.76 m and σ_c = 1.6 MPa as given above, the global ice force against the struc-

ture is estimated to be 291 MN or $\approx$ 3.24 MN/m. Since most estimates for the integrated limiting pack ice force lie between 10^4 and $10^5\ N/m$ (Parmerter and Coon 1973, Rothrock 1975, Hibler 1980, Nevel 1983 and Croasdale 1984), the pack ice driving force would seem to be the design limiting-force load. However, since the pack ice driving force can be distributed across a floe that is much wider than the structure, the concentrated force at the structure can easily exceed the stress required to fail the ice. Therefore, for this model and no other factors being considered, the design force would be the calculated value.

The constants given in eq 15 and 16 are best estimates and may need to be revised (Sanderson 1988). The estimated force of 291 MN is considered an upper limit for the conditions given. Indeed, for a similar ice sheet thickness and structure width, the ice force developed against the structure due to nonsimultaneous ice crushing failure appears to be less than half the above calculated indentation force (Wright and Timco 1994).

SUMMARY

A constitutive relationship, in the form $\sigma_c = B_2\ \dot{\varepsilon}^{1/n}\ \phi_B^m$, was developed for predicting the unconfined compressive strength of first-year sea-ice floes as a function of only two parameters, the applied strain rate and the ice floe bulk porosity. This equation was evaluated using full sea-ice sheet thickness, horizontal unconfined compression test data, so no uncertain small- to large-scale scaling laws were involved. The magnitudes of the parameters in the equation were found to be $\sigma_c = 2.7 \times 10^{-3}\ \dot{\varepsilon}^{1/3}\ \phi^{-1}$. Using this relationship, an example is given for estimating the design sea-ice crushing force against a 90-m-wide offshore structure.

Relationships are also provided for determining ice sheet tensile and flexural strength. The relation between sea-ice bulk conductivity and strength was explored. First-year sea-ice thickness can currently be measured using surface or airborne systems. It is predicted that one day ice sheet conductivity will also be remotely measured and that this will lead to the capability of remotely estimating sea-ice strength.

Two widely used methods for calculating the

15

brine volume of sea ice were discussed. Both methods were found to provide similar results, provided due diligence is exercised when making the required supporting measurements.

LITERATURE CITED

Anderson, D.L. (1961) Growth rate of sea ice. *Journal of Glaciology,* **3**(30): 1170–1172.

Cox, G.F.N. and W.F. Weeks (1974) Salinity variations in sea ice. *Journal of Glaciology,* **13**(67): 109–120.

Cox, G.F.N. and W.F. Weeks (1983) Equations for determining the gas and brine volumes in sea-ice samples. *Journal of Glaciology,* **29**(102): 306–316.

Croasdale, K.R. (1984) The limiting driving force approach to ice loads. In *Proceedings of the 16th Offshore Technology Conference, 7–9 May, Houston, Texas,* vol. 2, p. 57–64.

Dykins, J.E. (1970) Ice engineering: Tensile properties of saline ice grown in a confined system. NCEL Technical Report R-720. Port Hueneme, California: U.S. Naval Civil Engineering Laboratory.

Fish, A.M. (1993) Combined creep and yield model of ice under multiaxial stress. *Journal of Offshore and Polar Engineering,* **3**(2): 130–138.

Frankenstein, G. and R. Garner (1967) Equations for determining the brine volume of sea ice from –0.5° to –22.9°C. *Journal of Glaciology,* **6**(48): 943–944.

Gavrilo, V.P., S.M. Kovalev, G.A. Lebedev and O.A. Nedoshivin (1995) A method for estimating sea ice flexural strength based on hydrometeorological data. In *Proceedings of the 5th International Offshore and Polar Engineering Conference, The Hague, The Netherlands* (J.S. Chang, M. Sayed and A.M. Gresnigt, Eds.), vol. 2, p. 521–528. Golden, Colorado: International Society of Offshore and Polar Engineers (ISOPE).

Glen, J.W. (1955) The creep of polycrystalline ice. *Proceedings of the Royal Society, (London),* **228A**(1175): 519–538.

Glen, J.W. (1958) The flow law of ice. In *Proceedings of the Chamonix Symposium, 16–24 June, September.* IASH Publication 47, p. 171–183. Gentbrugge, Belgium.

Hibler, W.D. III (1980) Modeling a variable thickness sea ice cover. *Monthly Weather Review,* **108**(12): 1943–1973.

Kovacs, A. (1993) Axial double-ball test versus the uniaxial unconfined compression test for mea-suring the compressive strength of freshwater and sea ice. USA Cold Regions Research and Engineering Laboratory, CRREL Report 93-25.

Kovacs, A. (1996) Sea ice: Part I: Bulk salinity vs. ice floe thickness. USA Cold Regions Research and Engineering Laboratory, CRREL Report 96-7.

Kovacs, A., D. Diemand and J.J. Bayer, Jr. (1996) Electromagnetic induction sounding of sea ice thickness. USA Cold Regions Research and Engineering Laboratory, CRREL Report 96-6.

Kovacs, A. and J.S. Holladay (1990) Sea ice thickness measurement using a small airborne electromagnetic sounding system. *Geophysics,* **55**(10): 1327–1337

Kovacs, A. and R.M. Morey (1987) Electromagnetic measurements of a second-year sea ice floe. In *Proceedings of the 9th Conference on Port and Ocean Engineering Under Arctic Conditions (POAC–87), 17–21 August, University of Alaska, Fairbanks* (W.M Sackinger and M.O. Jeffries, Eds.), vol. 1. Fairbanks: Geophysical Institute, p. 121–136.

Kovacs, A. and R.M. Morey (1991) Sounding of sea ice thickness using a portable electromagnetic induction instrument. *Geophysics,* **54**(12): 1992–1998.

Kovacs, A., R.M. Morey and G.F.N. Cox (1987) Modeling the electromagnetic property trends in sea ice, Part I. *Cold Regions Science and Technology,* **14**(3): 207–235.

Kovacs, A., W.F. Weeks and F. Michitti (1969) Variation of some mechanical properties of polar snow, Camp Century, Greenland. USA Cold Regions Research and Engineering Laboratory, Research Report 276.

Mellor, M. (1986) Mechanical behavior of sea ice. In *Geophysics of Sea Ice* (N. Untersteiner, Ed.). New York: Plenum Press, p. 275–281.

Nevel, D.E. (1983) Pressure ridge forces. In *Proceedings of the 7th International Conference on Port and Ocean Engineering Under Arctic Conditions, Espoo, Finland.* Technical Research Center of Finland, vol. 1, p. 212–220.

Norton, H.F. (1929) *Creep of Steel at High Temperatures.* New York: McGraw-Hill.

Parmerter, R.R. and M.D. Coon (1973) Model of pressure ridge formation in sea ice. *Journal of Geophysical Research,* **77**(13): 6565–6575.

Rothrock, D.A. (1975) The energetics of the plastic deformation of pack ice by ridging. *Journal of Geophysical Research,* **80**(33): 4514–4519.

Sanderson, T.J.O. (1988) *Ice Mechanics: Risks to Offshore Structures.* London: Graham and Trotman.

Timco, G.W. and R.M.W. Frederking (1990) Compressive strength of sea ice sheets. *Cold Regions Science and Technology,* **17**(3): 227–240.

Timco, G.W. and S. O'Brien (1994) Flexural strength equation for sea ice. *Cold Regions Science and Technology,* **22**(3): 285–298.

Wen, T., G.R. Garrison, R.E. Francois, R.P. Stein and W.J. Felton (1991) Sound speed, reflectivity, and absorption measurements in Arctic ice in 1988. Applied Physics Laboratory, University of Washington, Technical Report APL-UW-TR-9005.

Wright, B.D. and G.W. Timco (1994) A review of ice forces and failure modes on the *Molikpaq*. In *Proceedings of the 12th IAHR Symposium on Ice, 23–26 August, Trondheim, Norway.* International Association of Hydraulic Research, vol. 2, p. 816–825.

REPORT DOCUMENTATION PAGE	Form Approved OMB No. 0704-0188

Public reporting burden for this collection of information is estimated to average 1 hour per response, including the time for reviewing instructions, searching existing data sources, gathering and maintaining the data needed, and completing and reviewing the collection of information. Send comments regarding this burden estimate or any other aspect of this collection of information, including suggestion for reducing this burden, to Washington Headquarters Services, Directorate for Information Operations and Reports, 1215 Jefferson Davis Highway, Suite 1204, Arlington, VA 22202-4302, and to the Office of Management and Budget, Paperwork Reduction Project (0704-0188), Washington, DC 20503.

1. AGENCY USE ONLY (Leave blank)	2. REPORT DATE September 1996	3. REPORT TYPE AND DATES COVERED

4. TITLE AND SUBTITLE	5. FUNDING NUMBERS
Sea Ice: Part II. Estimating the Full-Scale Tensile, Flexural, and Compressive Strength of First-Year Ice	

6. AUTHORS

Austin Kovacs

7. PERFORMING ORGANIZATION NAME(S) AND ADDRESS(ES)	8. PERFORMING ORGANIZATION REPORT NUMBER
U.S. Army Cold Regions Research and Engineering Laboratory 72 Lyme Road Hanover, New Hampshire 03755-1290	CRREL Report 96-11

9. SPONSORING/MONITORING AGENCY NAME(S) AND ADDRESS(ES)	10. SPONSORING/MONITORING AGENCY REPORT NUMBER
U.S. Army Cold Regions Research and Engineering Laboratory 72 Lyme Road Hanover, New Hampshire 03755-1290	

11. SUPPLEMENTARY NOTES
For conversion of SI units to non-SI units of measurement consult ASTM Standard E380-93, *Standard Practice for Use of the International System of Units*, published by the American Society for Testing and Materials, 1916 Race St., Philadelphia, Pa. 19103.

12a. DISTRIBUTION/AVAILABILITY STATEMENT	12b. DISTRIBUTION CODE
Approved for public release; distribution is unlimited. Available from NTIS, Springfield, Virginia 22161	

13. ABSTRACT (*Maximum 200 words*)

Sea-ice salinity, density, and temperature data were used to develop new methods for determining the bulk brine volume and porosity of sea-ice floes. Methods for estimating full-thickness ice sheet strength, based on large-scale field tests, are presented. The relationships among bulk sea-ice properties, strain rate, and strength are illustrated. A new constitutive equation was developed for predicting the full-thickness horizontal compressive strength σ_c of first-year sea ice as a function of the applied strain rate and bulk porosity in the form $\sigma_c = B_2 \dot{\varepsilon}^{1/n} \phi_B^m$, where parameters B_2, n, and m are about 2.7×10^3, 3, and -1, respectively, and $\dot{\varepsilon}$ and ϕ_B are the ice strain rate and ice floe bulk porosity of sea ice, respectively. An estimate of the horizontal force that may develop between first-year sea ice and a 90-m-wide structure is given. Estimating sea-ice strength based on remote ice conductivity measurements is also discussed conceptually.

14. SUBJECT TERMS				15. NUMBER OF PAGES 26
Porosity	Salinity	Sea ice	Strain rate	16. PRICE CODE

17. SECURITY CLASSIFICATION OF REPORT	18. SECURITY CLASSIFICATION OF THIS PAGE	19. SECURITY CLASSIFICATION OF ABSTRACT	20. LIMITATION OF ABSTRACT
UNCLASSIFIED	UNCLASSIFIED	UNCLASSIFIED	UL

NSN 7540-01-280-5500

Standard Form 298 (Rev. 2-89)
Prescribed by ANSI Std. Z39-18
298-102